Analysis and Design of Post-Regulation Stages for Resonant Capacitively-Coupled Wireless Power Systems

Eli Abramov, *Student Member*, *IEEE*, Yotam Schultz, *Student Member*, *IEEE*, Michael Evzelman, *Member*, *IEEE*, and Mor Mordechai Peretz, *Member*, *IEEE*

The Center for Power Electronics and Mixed-Signal IC, Department of Electrical and Computer Engineering
Ben-Gurion University of the Negev P.O. Box 653, Beer-Sheva 8410501, Israel
eliab@post.bgu.ac.il, shcultzy@ post.bgu.ac.il, evzelman@bgu.ac.il, morp@bgu.ac.il
http://www.ee.bgu.ac.il/~pemic

2022 IEEE Applied Power Electronics Conference and Exposition (APEC) | 978-1-6654-0688-8/22/$31.00 ©2022 IEEE | DOI: 10.1109/APEC43599.2022.9773472

***Abstract* — This study introduces a power regulation design methodology for power receiving units (PRUs) in capacitively-coupled resonant wireless power transfer (RWPT) systems by using hybrid multi-level (HML) post-regulators. A generic design framework for capacitive RWPT systems with post-regulation stages is developed, followed by a simplified behavioral model for the PRU including the additional regulation stage. It has been demonstrated that by using HML stages for power-regulation, significantly wider impedance matching range can be achieved, which results in better spatial freedom of wireless power systems. This study also covers design tradeoffs between several post-regulators in terms of efficiency, coupling range and conversion range. A 40 W experimental resonant capacitively-coupled WPT system with HML buck (HMLB) post-regulator has been designed and examined up to 150 mm misalignment, at a resonant operation of 3 MHz. A very good agreement is obtained between the theoretical predictions and experimental results.**

***Keywords* — closed-loop wireless system, impedance matching, resonant power transfer, post-regulation.**

I. Introduction

As the field of wireless power technology advances and adds more innovative uses, the need for both extended power periods and spatial freedom is rapidly increasing in many applications such as portable electronics, virtual and augmented reality, autonomous robots, drones etc. [1]-[9]. Although wireless power transfer (WPT) technology enables to extend the power periods and reduce the use of bulky batteries (in some cases even eliminate), truly spatial freedom, i.e., 3-Dimenssional movement is highly dependent on the coupling method and on the system's power-regulation capabilities [1]-[3].

In the context of dynamic WPT applications consuming low to high power (several watts up to kilo-watts), resonant-based WPT methods are in favor, since in overall, they enable better power transfer characteristics such as: spatial freedom, distance and power levels [4]-[10]. However, from practical point-of-view the latter is not sufficient, since for most applications the output power (voltage, current or both) should be well regulated, regardless of the medium variations. State-of-the-art power-regulation methods for wireless power receiving units (PRUs) are classified into three types: 1) passive regulation, 2) active rectification, 3) post-regulation stage [11].

Passive regulation which is based on the resonant network configuration is a simple straightforward approach, such that by proper resonant network design, constant voltage or current can be obtained at the output [12]-[14]. However, for industrial and commercial applications that require some spatial freedom this method is very limited, since in practice wireless power transfer systems suffer from variations of the wireless medium, electrical circuits and the resonators. In addition, passive power-regulation is not suitable for applications with load transitions such as: smart phones, laptops, tablets, etc.

The next regulation method which is based on active rectification of the AC-DC rectifier, i.e., controlling the conduction time of the power switches. As a result, the amount of current delivered to the load is controlled, thus, regulation at the output is obtained. Although, this approach enables single stage regulation without compromising too much the overall efficiency [15]-[18], since resonant-based WPT systems typically operate at the multi-MHz range within the industrial-scientific-medical (ISM) band: 6.78 MHz, 13.56 MHz, 27.12 MHz [19], the design efforts on the sensing circuitries and controller can be quite complex and tedious. Moreover, the requires that the rectifier's power switches are high-performance wide band-gap (WBG) devices such as silicon carbide (SiC) and gallium nitride (GaN), which results in higher costs and for some cases in labor intensive design efforts, particularly if the end-use application consumes medium to high power levels.

The final approach for regulating power in wireless applications is post-regulation stage, in which, the rectifier stage is cascaded by a low dropout (LDO) regulator or DC-DC converter [11], [20]-[22]. LDO regulator is a simple both cost and area effective approach that can provide precise voltage regulation, while maintaining relatively small voltage ripple at the output. Another advantage of LDO approach is that it can integrated with the PRU's controller into a single power system-on-chip (PSoC). However, for significant voltage (and power) levels, LDO regulator is limited by its voltage-current ratings, power conversion efficiency, and its overall dynamics. This can be improved by using a DC-DC post-regulation stage (e.g. buck, boost, buck-boost). Post-regulator is the closest to

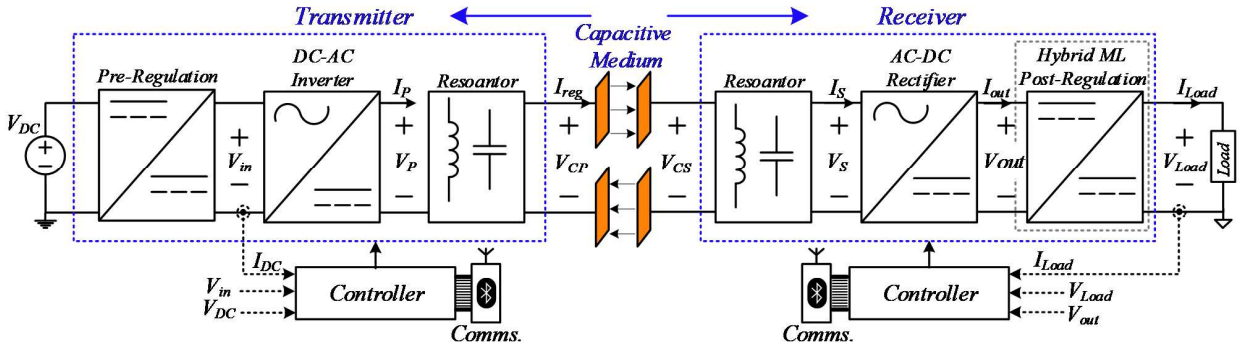

Fig. 1. Simplified block diagram of a controlled RWPT system with hybrid multi-level post-regulator at the PRU.

point-of-load (PoL), with significantly better dynamics compared to other methods. For battery-based and current-controlled commercial applications, DC-DC post-regulators are the only candidates that can satisfy the strict demands for precise load current regulation [11], [15]. Aside from impedance matching for regulating the target power to the load, post-regulators can be also used for maximum efficiency tracking in the PRU [22], [23], where specific equivalent impedance is required. Although DC-DC post-regulators are one of the main enablers for improving the spatial freedom in WPT applications, at extreme misalignments and medium variations (coupling coefficient variations), in which wider compensation range is required, which translates to higher conversion ratios, conventional post-regulators introduce significant losses, reducing the overall end-to-end efficiency of the WPT system.

Hybrid multi-level (HML) topologies provide large step-down/up conversions ratios, while maintaining higher efficiency and power density compared to conventional DC-DC converters [24]-[28]. This comes at the cost of additional switches and passive components, however, in the context of very-high conversion ratios the overall volume is not compromised too much compared to conventional converters (assuming same operating conditions are employed). To-date, framework for analysis and design of post-regulation stages have not been addressed in the context of wireless power systems. *It would be extremely beneficial if such design framework for WPT is utilized, since both the steady-state and the dynamic characteristics of the post-regulation stage are tightly coupled with the WPT stage.*

The objective of this study is, therefore, to introduce detailed analysis of resonant-based capacitive WPT systems with post-regulation stages with emphasis on HML topologies, as shown in Fig. 1. The analysis followed by simplified behavioral models of the system, further simplifying the design of an end-to-end capacitive WPT system. The analysis methodology is to explore the affecting factors on the power-regulation conditions, and consequently, outline the design guidelines on the post-regulation stage for wireless power systems. Based on the design framework, this study also covers comprehensive comparison between conventional and HML post-regulators in capacitive RWPT. It is a further objective of this study to design and investigate the performance and characteristics of a capacitively-coupled RWPT system with HML buck (HMLB) post-regulator under various operating conditions.

The rest of the paper is organized as follows: Following a brief survey of capacitive RWPT system with LC resonator, Section II describes the equivalent impedances reflection in the PRU. Section III presents a case-study of a capacitive system with HMLB post-regulation stage, followed by comparison between several post-regulation stages. Section IV provides an experimental validation of the theoretical analysis through a capacitive RWPT prototype. Section V concludes the paper.

II. Characteristics of Resonant-Based Capacitive WPT Systems

To facilitate the framework for the analysis of a capacitive wireless power system with post-regulation stage, first, this section briefly describes and reviews capacitive RWPT systems with double-sided LC resonant converter configuration [6], [29]. Only the essential in-context details have been brought up here in order to establish the for an end-to-end system analysis. Then, the relationships between the receiver's output stages are covered through equivalent reflected impendence per stage.

A. Review of LC-Based Capacitive RWPT Systems

A capacitively-coupled WPT system with LC resonators in both the transmitter and receiver, where, the wireless medium is formed by two pairs of conductive coupling plates, such as copper foils or aluminum [6], [30], [31] is anlayzed. The capacitive medium can be modeled as π-type network [6], [32]. Assuming loosely-coupled operation, i.e., the coupling capacitances C_M, C_{M1}, C_{M2}, are relatively low compared to C_P and C_S [6], [12], [32] , the drive frequency, f_{INV}, is near the resonators natural frequency (i.e., $f_{INV} \approx f_0 = 1/(2\pi\sqrt{L_P C_P})$, $= 1/(2\pi\sqrt{L_S C_S})$, then the currents as well as voltages of the passive components are virtually sinusoidal [33]. This is since high-Q operation is naturally facilitated as the effective output impedance of the resonator in the transmitter is relatively high. Typical waveforms of the system are shown in Fig. 2a. As can be seen, while the transmitter and receiver voltages V_P and V_S are square waves, the currents are sinusoidal due to high-Q operation of the circuit. Since a full-bridge inverter is used at the front-end, the transmitter voltage V_P toggles between $\pm V_{in}$, while the receiver voltage, V_S, toggles between $\pm V_{out}$. It can be also seen, that for both the transmitter and receiver sides the current is in phase with the voltage, whereas the receiver current I_S lags the transmitter current I_P by 90º (same applies for the voltages V_S and V_P). By employing first harmonic

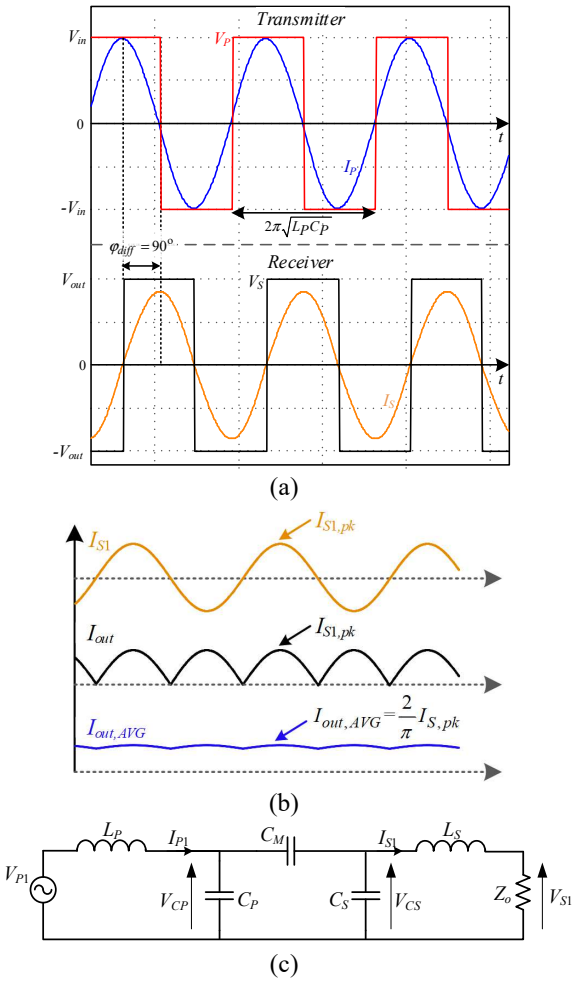

Fig. 2. Double-sided LC RWPT system (a) Typical currents and voltages waveforms of the capacitive RWPT system: upper signals - transmitter, bottom signals – receiver; (b) PRU currents waveforms; (c) Overall system model by employing first harmonic approximation.

approximation (FHA), and by utilizing the capacitive medium model, where V_{P1} and V_{S1} represent the first harmonics of the square waves V_P and V_S, and the magnitudes of the first harmonic are $4V_{in}/\pi$ and $4V_{out}/\pi$, respectively; Z_O is the reflected impedance with respect to the load such that $Z_O=\frac{8}{\pi^2}R_{Load}$. Fig. 2b shows the PRUs currents before and after the rectifier stage, where I_{S1} is the current of the first harmonic. Assuming I_{out} is filtered by an output capacitor, the average output current and voltage are

$$\begin{cases} I_{out,AVG}=\dfrac{2}{\pi}I_{S1,PK} \\ V_{out,AVG}=\dfrac{\pi}{4}V_{S1,PK} \end{cases}, \tag{1}$$

Based on the above relationships, the overall system can be modeled as shown in Fig. 2c. It should be noted that the above outcomes, are obtained under the assumption that the transmitter and receiver are resonating at the same frequency.

B. Equivalent Impedance Reflection

Fig. 3 shows a simplified schematic diagram of the PRU output stages. Assuming steady-state conditions, the post-regulation can be considered as a three-port stage comprising:

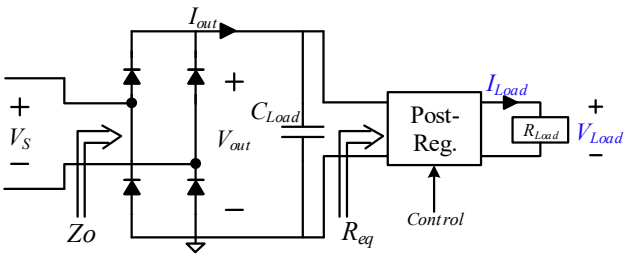

Fig. 3. Schematic diagram of the PRU output stages with notation of the reflected impedances.

input power, output power, control signal, such that the output voltage can be represented in a generic form as follows [34]

$$V_{Load}=M(D)\cdot V_{out}, \tag{2}$$

where V_{out} is the voltage after the rectifier stage, and $M(D)$ is the conversion ratio of the post-regulator at steady-state, and it is a function of the duty-cycle, $d(t)$. Therefore, by taking into consideration the efficiency factor in such regulators, it can be assumed that the generic form of the output current is

$$I_{Load}=\frac{I_{out}}{M(D)}\eta, \tag{3}$$

where I_{out} is the current after the rectifier stage and η is the efficiency of the regulator. By applying (2) into (3), the equivalent input resistance of the pos-regulator can be expressed as

$$R_{eq}=\frac{V_{out}}{I_{out}}=\frac{V_{Load}}{I_{Load}M^2(D)}\eta=\frac{R_{Load}}{M^2(D)}\eta, \tag{4}$$

and by using the FHA relationships discussed in the previous section, the reflected impendence seen from the input of the rectifier stage, Z_O, can be expressed with respect to the load and the conversion ratio as follows

$$Z_O=\frac{8}{\pi^2}R_{eq}=\frac{8}{\pi^2}\frac{R_{Load}}{M^2(D)}\eta. \tag{5}$$

Z_O can be also expressed in a straightforward manner as

$$Z_O=\frac{{V_{S1}}^2}{2P_O}\Rightarrow {V_{S1}}^2=2Z_OP_O, \tag{6}$$

where $P_O=P_{Load}/\eta$ and it is the equivalent power of Z_O.

From (5) and (6) it can be seen that for given target output power and finite efficiency of the post-regulation, wider range of $M(d)$ enables wider range of Z_O, i.e., better compensation for V_S variations, which are primarily due to medium variations and the cross-coupling relationships between the transmitter and receiver, as will be discussed in detail in the following section.

III. Capacitive RWPT with Hybrid Multi-Level Buck Post-Regulator

Following the observations and derivations made in the previous section, a capacitively-coupled double-sided LC RWPT system with a wide-input step-down HMLB post-regulation stage is analyzed (Fig. 4). The HMLB converter has several distinguishing advantages over the conventional buck converter [26]. First, assuming charge balance across the flying capacitor, C_f, is maintained, the voltage swing at the switching

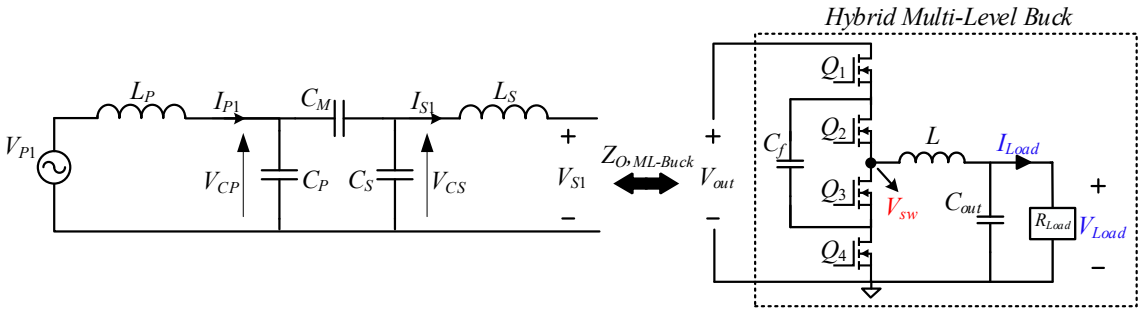

Fig. 4. FHA schematic diagram of a capacitive RWPT system with hybrid multi-level buck post-regulation stage.

node is half of the input voltage, which in the context of the WTP system, is half of the rectified voltage of V_S. Next, the effective switching frequency ($1/T_{SW,eff}$) at the switching node, V_{SW}, is twice the switching frequency $f_{SW} = 1/T_{SW}$. These translates to better power density and less efforts on the overall heat dissipation of the converter. In addition, in a conventional buck converter, due to the blocking voltage, V_{ds}, requirement of the switches [26], [34], both of the switches need to be rated for maximum input voltage of V_S. Although in the multi-level buck there are four switches, these switches can be rated for $V_S/2$, since silicon area for switch realization is approximately proportional to V_{ds}^2, the overall semiconductor areas of multi-level and conventional buck converters can be equivalent [26], [35]. Furthermore, typically the volume of the output filter is significantly larger than that of the semiconductor components, which in the case of the HMLB due to the combined reduction of the voltage swing at the switching node, and two times higher effective switching frequency, the output filter is further reduced, thus, the additional switches virtually does not introduce volumetric penalty [36]. From control perspective, the multi-level buck does not require any additional peripherals, and the core control is the same as for the conventional buck, with potentially improved dynamics.

Typical waveforms of the multi-level buck at steady-state are depicted in Fig. 5, there, the operation of the converter is divided into four switching phases, in which, Q_1 and Q_4 are complementary, Q_2 and Q_3 are also complementary, and Q_2 is delayed from Q_1 in $T_{SW}/2$. It can be seen that for a case that $V_{Load} < V_S/2$ (Fig. 5a), the switching node toggles between 0 to $V_S/2$; for $V_{Load} = V_S/2$ (Fig. 5b), neglecting the flying capacitor charge balance mismatches, the switching node is virtually constant and equals to $V_S/2 = V_{Load}$, and the inductor current is also virtually constant $I_L = I_{Load}$; for $V_S/2 < V_{Load} < V_S$ (Fig. 5c) the switching node toggles between $V_S/2$ to V_S. As discussed above, it can be observed that for the entire operation region, the maximum voltage drop over the inductor (and the switches) is $V_S/2$.

The conversion ratio function, $M(D)$, of the HMLB converter is identical to the conventional buck and it equals to $d(t)$. Thus, by using (5), the equivalent reflected impudence of the multi-level buck, $Z_{O,ML\text{-}Buck}$, is

$$Z_{O,ML-Buck} = \frac{8}{\pi^2}\frac{R_{Load}}{d^2}\eta \,. \tag{7}$$

From (7), the duty ratio can be calculated

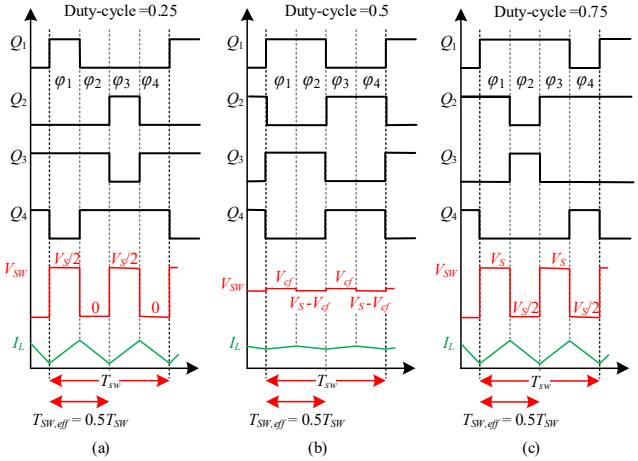

Fig. 5. Gate signals, switching node and inductor waveforms of the post-regulator for duty-cycle of: (a) d=0.25, (b) d=0.5, d=0.75.

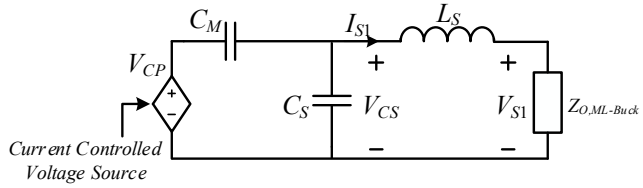

Fig. 6. Behavioral model of the PRU while the transmitter is current-controlled.

$$d = \sqrt{\frac{8}{\pi^2}\frac{R_{Load}}{Z_{O,ML-Buck}}\eta} \,. \tag{8}$$

One of the methods to control transmitters in RWPT systems, and in particular in multi-receiver RWPT systems, is by constant current regulation [11], [19], [37]. By employing such control approach on the analyzed capacitive system, the voltage V_{CP} can be treated constant, therefore, the circuit in Fig. 4 can be simplified to the circuit shown in Fig. 6. By applying Kirchhoff's voltage law on the circuit of Fig. 6, the voltage V_{CS} can be expressed as

$$\begin{cases} V_{CS} = V_{CP}\dfrac{Z_S}{Z_S + Z_{CM}} \\ Z_S = Z_{CS} \parallel \left(Z_{LS} + Z_{O,ML-Buck}\right) \\ Z_{CM} = 1/j\omega C_M \end{cases} . \tag{9}$$

The voltage V_{S1} can be expressed as

$$V_{S1} = V_{CS}\frac{Z_{O,ML-Buck}}{Z_{O,ML-Buck} + j\omega L_S}. \quad (10)$$

By substituting (9) into (10), and rearranging the expression, V_{S1} is expressed as

$$V_{S1} = V_{CP}\frac{Z_{O,ML-Buck}}{Z_{O,ML-Buck} + j\omega L_S + \dfrac{1-\omega^2 L_S C_S + j\omega C_S Z_{O,ML-Buck}}{j\omega C_M}}, \quad (11)$$

and if operation in resonance is assumed, V_{S1} can be simplified to

$$V_{S1} = V_{CP}\frac{Z_{O,ML-Buck}}{Z_{O,ML-Buck}\left(1 + {C_S}/{C_M}\right) + j\omega L_S}. \quad (12)$$

By substituting the expression in (6) into (12), and after some manipulations, V_{S1} can be further expressed as

$$V_{S1} = \frac{\dfrac{V_{CP}C_M}{C_M + C_S} + \sqrt{\left(\dfrac{V_{CP}C_M}{C_M + C_S}\right)^2 - j4\omega L_S}}{2}. \quad (13)$$

As mentioned in the previous sections, RWPT systems operate in the MHz range, thus, typically the resonators' capacitance values are in the range of hundreds of pF, inductances are tens to hundreds µH, and the mutual coupling capacitance, C_M, is in the order of a few pF. As a result, the expression in (13) can be simplified to generic expressions as follows

$$\frac{V_{CP}C_M}{C_M + C_S} >> 4\omega L_S \;\Rightarrow\; V_{S1} = \frac{V_{CP}C_M}{C_M + C_S}. \quad (14)$$

Having the relationships given in (6), (8) and (14), the duty ratio can be calculated for any operating point as a function of the operating conditions of the transmitter, medium variations (translates to changes in C_M), and the PRU's resonator.

Using the above analysis and observations, generalized design guidelines to examine and design an end-to-end capacitive RWPT system with post-regulation stage are summarized as follows:

1) Given target/predicted values for transmitter's voltages and currents, medium characteristics, resonators values and resonant frequency.
2) Assume operation in resonance and extract the overall system model by employing FHA.
3) Given the target output power, substitute (6) into (12), and calculate V_{S1}.
4) Use V_{S1} to calculate Z_O from (6).
5) Given nominal operating point, based on the chosen post-regulator, insert the predicted efficiency η, $M(d)$, and Z_O to (5), and calculate the duty-cycle d.
6) Examine the duty-cycle ranges and post-regulator performance for corner operating points of the RWPT system.

To further highlight the advantages of the HMLB as a post-regulation stage, given the operating conditions summarized in Table I, a more thorough comparison between buck and multi-level buck over wide range of the coupling capacitance has been carried out, as shown in Fig. 7. First, for various duty-cycles, rigors loss estimation has been done for both topologies. It can be seen that for the given RWPT system, at extremely weak coupling (C_M <6 pF), in terms of efficiency, conventional buck converter has reasonable efficiency over 91%. However, as the operating points move toward the strongly-coupled region (C_M >14 pF), where high-conversion ratios are required, the efficiency of the buck converter drops below 80%, whereas the HMLB remains above 80% efficiency up to C_M ≈40 pF. It should be noted that the blocking voltage of the chosen switches for both converters is Vds=100 V, thus, in practice for the given RWPT system regardless the efficiency criteria, the conversion range of the buck converter is limited to d=0.2, while the HMLB can be potentially pushed to 0.1 duty-cycle. It should be further emphasized that by compromising on the operation range such that 0.35≤ d ≤0.9, the switches of the buck converter can be optimized with lower blocking voltage Vds=60, resulting in better efficiencies (similar to the HMLB) as illustrated by the dashed line in Fig. 7.

TABLE I – SIMULATION TEST-BENCH VALUES AND PARAMETERS AT NOMINAL OPERATION

Parameter	*Value/Type*
Input voltage V_{in}	20.5 V
Transmitter resonator	20.8 µH, 120 pF
Receiver resonator	21.6 µH, 130 pF
Resonant frequency f_0	3 MHz
Coupling capacitance C_M	14 pF
Load resistance R_{Load}	10 Ω
Output capacitor C_{Load}	90 µF
Output inductor L	10 µH
Flying capacitor C_{fly}	10 µF
Post-regulator switching frequency f_{SW}	250 kHz (500 kHz effective)
Load voltage V_{Load}	20 V
Load power P_{Load}	40 W

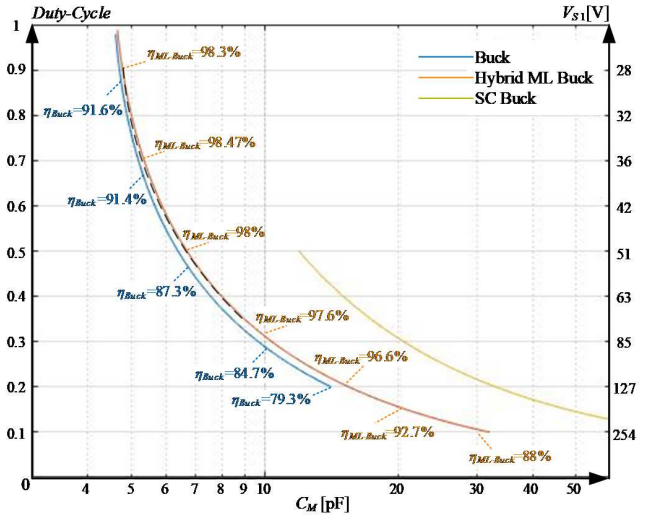

Fig. 7. Conversion ratio ranges of different post-regulators for the analyzed RWPT system.

To exemplify more design considerations of post-regulators in WPT, Fig. 7 also depicts the conversion range of a series-capacitor (SC) buck converter [28]. For sake of simplicity, the parameters of the SC buck are same as for the previous converters, and by using the expression in (5), the duty ratio for the SC buck can be expressed as follows

$$d_{SC-Buck} = \sqrt{\frac{32}{\pi^2}\frac{R_{Load}}{Z_O}\eta}. \quad (15)$$

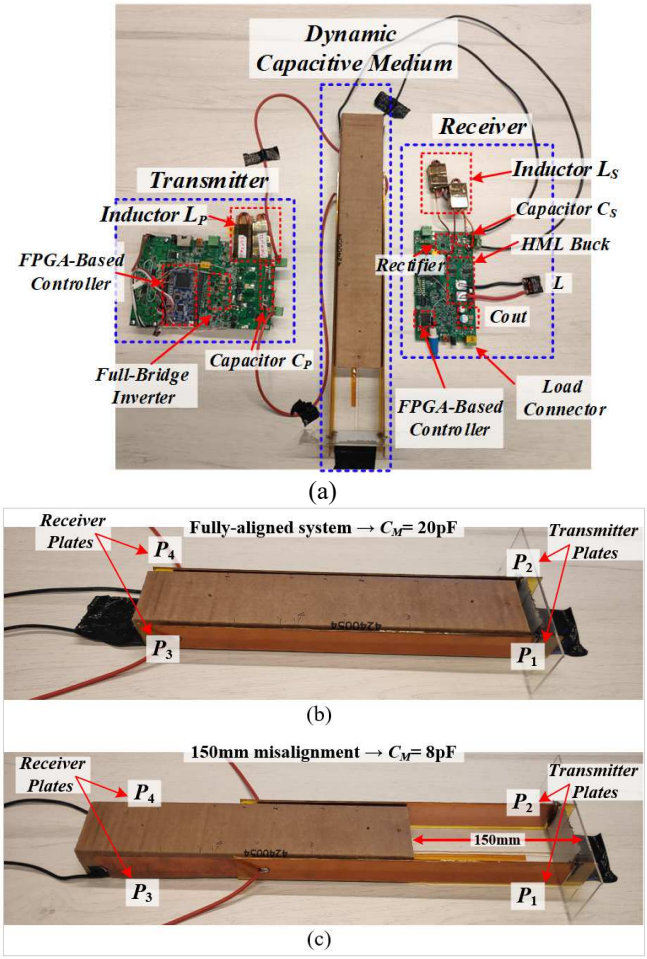

Fig. 8. (a) Resonant capacitively-coupled WPT experimental setup; Zoom-in views on the capacitive-coupler for: (b) fully-aligned system, C_M=20 pF; (c) 150 mm misalignment, C_M=8 pF.

Although SC buck is limited to maximum 50% duty-cycle, it can be seen that if the system is operated at C_M >15 pF while maintaining significantly wider operating range, SC buck would be the better candidate to perform such post-regulation task.

IV. Experimental Verification

Based on the above analysis an experimental capacitively-coupled double-sided LC RWPT system (Fig. 8a) with HMLB post-regulator has been designed and examined. The capacitive coupler has been designed to be symmetrical, where each coupling plate is made of copper stripe with overall dimensions of 300x30 mm. In addition, the capacitive coupler has been constructed to be dynamic, such that the wireless medium can be simply varied to different misalignments. Zoom-in view on the capacitive coupler for fully-aligned system and 150 mm misalignment are shown in Fig. 8 b and c, respectively. The RWTP system has been designed such that, L_P=21 µH, C_P=120 pF and L_S=22 µH, C_S=130 pF, at a resonance frequency $f_0 \approx 3$ MHz. The full-bridge inverter has been realized with EPC's 200-V enhancement mode GaN devices for multi-MHz operation [38]. The controller for the transmitter has been implemented on DE0-Nano Cyclone IV FPGA [39]. The PRU was digitally controlled using a MAX-10 FPGA [40] using fully digital high-performance control peripherals as detailed in [41]. Table I summarizes the components values and parameters of the experimental setup.

TABLE II – Capacitive RWPT Experimental Setup Values and Parameters

Parameter	*Value/Type*
Nominal input voltage V_{in}	35 V
Transmitter regulated current	~2.5-A peak
Transmitter resonator	21 µH, 120 pF, AVX MLLC 3 kV
Receiver resonator	22 µH, 130 pF,AVX MLLC 3 kV
Resonant frequency f_0	3 MHz
Nominal Coupling capacitance C_M	14 pF
Capacitive medium	300x30 mm, copper stripes
Medium misalignment	Up to 150 mm
Full-bridge inverter	200 V, EPC 2034
Rectifier diodes	200 V, CDBZ320200-HF
Load voltage V_{Load}	20 V
Load power P_{Load}	40 W
Load resistance R_{Load}	10 Ω, BK Precision electronic load
Output capacitor C_{Load}	68 µF, 80 V, 28 mΩ ESR, FPCR1K680MCL1GS
Output inductor L	12 µH, 3 mΩ DCR, SER2211-123MED
Flying capacitor C_{fly}	8.8 µF, 100 V, 2 mΩ ESR, 12101C335K4T2A
Post-regulator switching frequency f_{SW}	~250 kHz (500 kHz effective)
HML buck MOSFETs	100 V, 9.6 mΩ, BSZ096N10LS5

The resonant WPT system has been examined for 40 W load output power, at 75 mm misalignment, which translates to ~14 pF (Fig. 9a), such that the transmitter's resonant current, I_P, is regulated to 2.5 A peak, and the voltage V_P toggles between -35 and 35 V. The rectifier voltage at the receiver side, V_S, toggles between -90 and 90 V, while the current, I_S, peaks at 1 A. Fig. 9b shows the main waveforms of the HMLB at steady-state operation. It can be observed that load voltage is 20 V, the effective switching frequency is ~500 kHz, and the effective duty-cycle is 22.4% (half of the duty ratio of the switching node).

To further validate the design methodology, the system has been examined for medium variations on-the-fly. Figs. 10a and 10b shows experimental measurements for step-up in the medium, i.e., from 75 mm misalignment to fully aligned coupler, which translates to coupling variation of 14 pF to 20 pF. Fig. 10a depicts PRU's main waveforms without post-regulator, it can be seen that after variation of the coupler both the V_S and I_S increase to peak values of 115 V and 1.5 A, respectively. This results in load output power ~85 W, approximately twice than the target load power. On the other hand, Fig. 10b shows the PRU's main waveforms with post-regulations stage. Although V_S has not change much, it can be seen the I_S drops by 20%, and the load power is well regulated to 40 (resulting in effective duty-cycle ~ 16.66%). The system has been also examined for step-down variation from 75 mm to 150 mm (14 pF to 8 pF). It can be seen in Fig. 10c that without post-regulation the load power drops by a factor of two to the range of 20 W, while for the regulated system (Fig. 10d) the target load power is preserved (resulting in effective the duty-cycle ~ 37%), which is in good agreement with the theoretical predictions.

V. Conclusions

A power regulation methodology for PRUs in capacitive RWPT systems by means of HML post-regulation stages with wide impedance matching range has been presented. Comprehensive design framework for capacitive RWPT systems with post-regulation stages has been introduced, followed by simplified models of the overall system with emphasis on the PRU. Based on the design guidelines, an LC-based capacitive wireless power system with HMLB converter has been analyzed and examined. It has been shown that

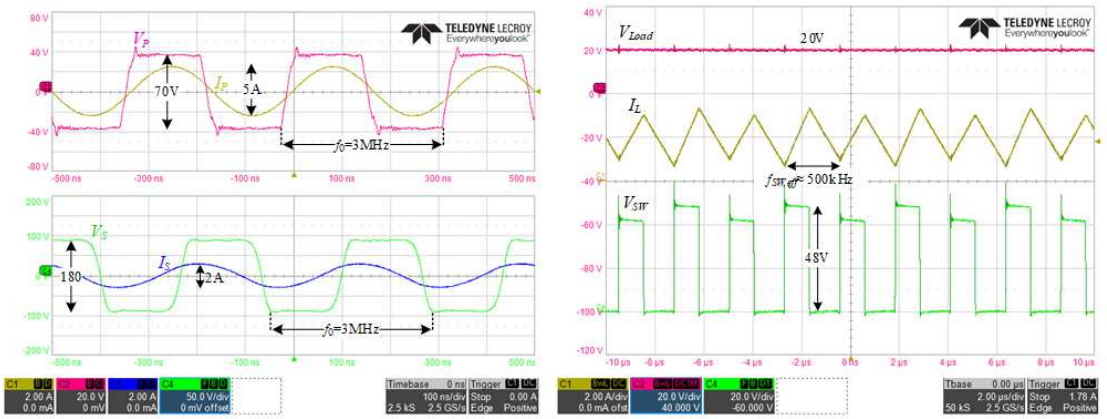

(a) (b)

Fig. 9. Experimental results of the system at 75mm (C_M≈14 pF) misalignment: (a) transmitter and receiver main waveforms; (b) post-regulator main.

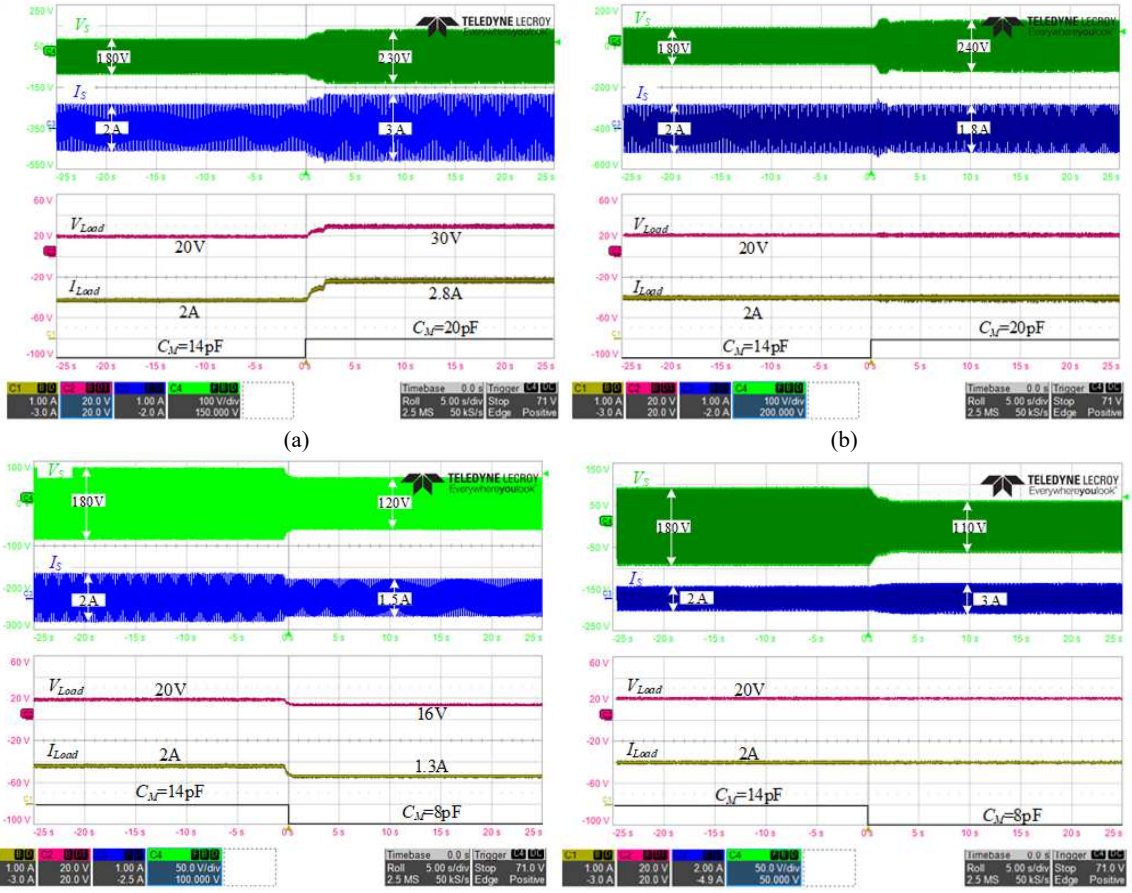

(a) (b)

(c) (d)

Fig. 10. Experimental measurements of the capacitive RWPT system for step-up medium variation, 14 pF to 20 pF: (a) receiver main waveforms without post-regulation; (b) receiver main waveforms with post-regulation; (c) zoom-in view on the transmitter and receiver main waveforms with post-regulation at steady-state; (d) post-regulator main waveforms.

compared to the conventional buck converter, the HML stage is superior in terms of overall efficiency and compensation range, which translates to improved spatial freedom of wireless power systems. In addition, for the analyzed capacitively-coupled system a comparison between an HMLB and SC buck has been carried out. It has been shown that for the weak coupling regions HMLB is the better candidate, while for the strong coupling regions the SC buck converter provide significantly wider range.

To further validate the design methodology, an experimental capacitive RWPT prototype operating at 3 MHz has been constructed. The prototype has been evaluated at various operating points up to 150 mm misalignment and 40 W output power delivery. The experimental case study confirmed the theoretical predictions of the design and modeling approach with an excellent agreement between the analytical derivations and experimental results.

REFERENCES

[1] Z. Zhang, H. Pang, A. Georgiadis, and C. Cecati, "Wireless power transfer—An overview," *IEEE Trans. Ind. Electron*., vol. 66, no. 2, pp. 1044–1058, Feb. 2019.

[2] S. Y. R. Hui, "Wireless power transfer: A brief review & update," *in Power Electronics Systems and Applications (PESA)*, 2013 5th International Conference on, Dec 2013, pp. 1–4.

[3] M. P. Kazmierkowski and A. J. Moradewicz, "Unplugged but connected: Review of contactless energy transfer systems," *IEEE Industrial Electronics Magazine*, vol. 6, no. 4, pp. 47–55, Dec 2012.

[4] F. Musavi and W. Eberle, "Overview of wireless power transfer technologies for electric vehicle battery charging," *IET Power Electron*., vol. 7, no. 1, pp. 60–66, Jan. 2014.

[5] F. Lu, H. Zhang, C. Mi, "A two-plate capacitive wireless power transfer system for electric vehicle charging Applications," *IEEE Trans. Power Electron*, vol. 33, no. 2, pp. 946-969, Aug. 2017.

[6] F. Lu, H. Zhang, H. Hofmann, and C. Mi, "A double-sided LC compensation circuit for loosely-coupled capacitive power transfer," *IEEE Trans. Power Electron*., vol. 33, no. 2, pp. 1633 – 1643, Feb. 2017.

[7] A. Kurs, A. Karalis, R. Moffat, J. D. Joannopoulos, P. Fisher, and M. Soljacic, "Wireless power transfer via strongly coupled magnetic resonances," *Science*, vol. 317, no. 5834, pp. 83-86, July 2007

[8] J. Shin et al., "Design and implementation of shaped magnetic-resonance-based wireless power transfer system for roadway-powered moving electric vehicles," *IEEE Trans. Ind. Electron*., vol. 61, no. 3, pp. 1179–1192, Mar. 2014.

[9] X. Qu et al., "Wide design range of constant output current using double-sided LC compensation circuits for inductive-power-transfer applications," *IEEE Trans. Power Electron*., vol. 34, no. 3, pp. 2364–2374, Mar. 2019.

[10] Y. Zhang, and M. A. de Rooij, "How eGaN® FETs are enabling large area wireless power transfer," *IEEE Workshop on Wide Bandgap Power Devices and Applications* (*WiPDA*), October 2017, pp 366 – 372.

[11] Y. Liu, B. Li, M. Huang, Z. Chen, and X. Zhang, "An overview of regulation topologies in resonant wireless power transfer systems for consumer electronics or bio-implants", in *Energies*, vol. 11, no. 7, 1737, 2018.

[12] W. Zhang and C. Mi, "Compensation topologies for high power wireless power transfer systems," *IEEE Transactions on Vehicular Technology*, vol. 65, no.6, pp. 4768-4778, july 2015.

[13] Y. Lim, H. Tang, S. Lim, J. Park, "An adaptive impedance-matching network based on a novel capacitor matrix for wireless power transfer," *IEEE Transactions on Power Electronics*, vol. 29, no. 8, pp. 4403-4413, August 2014.

[14] T.C. Beh, M. Kato, T. Imura, S. Oh and Y. Hori, "Automated impedance matching system for robust wireless power transfer via magnetic resonance coupling," *IEEE Transactions on Industrial Electronics*, vol. 60, no. 9, pp. 3689-3698, September 2013.

[15] C. Kim, S. Ha, J. Park, A. Akinin, P. P. Mercier, and G. Cauwenberghs, "A 144-MHz fully integrated resonant regulating rectifier with hybrid pulse modulation for mm-sized implants," *IEEE J. Solid-State Circuits*, vol. 52, no. 11, pp. 3043–3055, Nov. 2017.

[16] H.-M. Lee, H. Park, and M. Ghovanloo, "A power-efficient wireless system with adaptive supply control for deep brain stimulation," IEEE J. Solid-State Circuits, vol. 48, no. 9, pp. 2203–2216, Sep. 2013.

[17] H. G. Park et al., "A design of a wireless power receiving unit with a high-efficiency 6.78-MHz active rectifier using shared DLLs for magnetic-resonant A4 WP applications," *IEEE Trans. Power Electron*., vol. 31, no. 6, pp. 4484–4498, Jun. 2016.

[18] E. Ozalevli et al., "A cost-effective adaptive rectifier for low power loosely coupled wireless power transfer systems," *IEEE Trans. Circuits Syst. I: Regular Papers*, vol. 65, no. 7, pp. 2318–2329, Jul. 2018.

[19] R. Tseng, B.V.Novak, S. Shevde, and K. A. Grajski, "Introduction to the alliance for wireless power loosely-coupled wireless power transfer system specification version 1.0," in *Proc. IEEE Wireless Power Transfer Conf.*, Perugia, Italy, May 15–16, 2013, pp. 79–83.

[20] K.-G. Moh, F. Neri, S. Moon, P. Yeon, J. Yu, Y. Cheon, Y.-S. Roh, M. Ko, and B.-H. Park, "A fully integrated 6W wireless power receiver operating at 6.78 MHz with magnetic resonance coupling," in *Proc. ISSCC*, 2015, pp. 230–232.

[21] Y. J. Park et al., "A triple-mode wireless power-receiving unit with 85.5% system efficiency for A4WP, WPC, and PMA applications," *IEEE Trans. Power Electron*., vol. 33, no. 4, pp. 3141–3156, Apr. 2018.

[22] H. Li, Y. Tang, K. Wang, and X. Yang, "Analysis and control of post regulation of wireless power transfer systems," in *Proc. IEEE 2nd Annu. Southern Power Electron. Conf*., 2016, pp. 1–5.

[23] H. Li, J. Li, K. Wang, W. Chen, and Y. Xu, "A maximum efficiency point tracking control scheme for wireless power transfer systems using magnetic resonant coupling," *IEEE Trans. Power Electron*., vol. 30, no. 7, pp. 3998–4008, Jul. 2015.

[24] Y. Lei, W. C. Liu, and R. C. N. Pilawa-Podgurski, "An analytical method to evaluate and design hybrid switched-capacitor and multilevel converters," in *IEEE Trans. Power Electron*., vol. 33, no. 3, pp. 2227–2240, Mar. 2017.

[25] Z. Liao, Y. Lei, and R. C. N. Pilawa-Podgurski, "Analysis and design of a high-power density flying-capacitor multilevel boost converter for high step-up conversion," in *IEEE Transactions on Power Electronics*, 2018.

[26] S. M. Ahsanuzzaman, Y. Ma, A. A. Pathan, and A. Prodic, "A low-volume hybrid step-down dc-dc converter based on the dual use of flying capacitor," in *Proc. IEEE Appl. Power Electron. Conf. Expo*., Mar. 2016, pp. 2497–2503.

[27] O. Kirshenboim and M. M. Peretz, "High-efficiency non-isolated converter with very high step-down conversion ratio," *IEEE Trans. Power Electron*., vol. 32, no. 5, pp. 3683–3690, May 2017.

[28] Y. Jang and M. M. Jovanovic, "Non-isolated power conversion system having multiple switching power converters," U.S. Patent Appl. 10/972,632, Oct. 26, 2004.

[29] X. Qu et al., "Wide design range of constant output current using double-sided LC compensation circuits for inductive-power-transfer applications," *IEEE Trans. Power Electron*., vol. 34, no. 3, pp. 2364–2374, Mar. 2019.

[30] M. P. Theodoridis, "Effective capacitive power transfer," *IEEE Trans. Power Electron*., vol. 27, no. 12, pp. 4906–4913, Dec. 2012.

[31] S. Sinha, A. Kumar, B. Regensburger, and K. K. Afridi, "A new design approach to mitigating the effect of parasitics in capacitive wireless power transfer systems for electric vehicle charging," *IEEE Trans. Transp. Electrific*., vol. 5, no. 4, pp. 1040–1059, Dec. 2019.

[32] C. Liu, A.P. Hu, and M. Budhia, "A generalized coupling model for capacitive power transfer systems," *Proc. 36th Annual Conf. on IEEE Ind. Electron. Society*, Glendale, AZ, pp.274–279, Nov. 2010.

[33] R.L. Steigerwald, "A comparison of half-bridge resonant converter topologies," *IEEE Transactions on Power Electronics*, vol. 3, no. 2, pp. 174-182, April 1988.

[34] Robert W. Erickson and Dragan Maksimović , "Fundamentals of power electronics", Second Edition, New York: Springer Science+Business Media, 2001.

[35] B. J. Baliga, "Fundamentals of power semiconductor devices", Springer Science, 2008.

[36] Y. Lei, W.C. Liu, and R. C. N. Pilawa, "An analytical method to evaluate flying capacitor multilevel converter and hybrid switched-capacitor converters for large voltage conversion ratios," in *Proc. IEEE Workshop on Control and Modeling for Power Electronics (COMPEL),* Aug. 2015.

[37] E. Abramov and M. M. Peretz, "Adaptive self-tuned mixed-signal controller IC for resonant wireless power transfer," in *IEEE Applied Power Electronics Conference and Exposition (APEC)*, March 2020, pp. 805-812.

[38] https://epcco.com/epc/Portals/0/epc/documents/datasheets/EPC2034_datasheet.pdf.

[39] DE0-Nano Development and Education Board user manual, terasIC Inc. - Intel, 2016.

[40] https://www.intel.com/content/dam/www/programmable/us/en/pdfs/literature/hb/max-10/m10_datasheet.pdf

[41] E. Abramov, T. Vekslender, O. Kirshenboim, and M. M. Peretz, "Fully-integrated digital average current-mode control voltage regulator module IC," *IEEE Journal on Emerging and Selected Topics in Power Electronics,* vol. 6, no. 2, pp. 549-562, Jun. 2018.